LOCAL SATURATION MEASUREMENT WHILE CENTRIFUGING (MWC) FOR IMPROVING CENTRIFUGE CAPILLARY-PRESSURE CURVE DETERMINATION.

P. Forbes, C. Chardaire-Rivière, F. Deflandre, M. Fleury, Institut Francais du Pétrole, 1-4 ave. de Bois Préau, 92500, Rueil-Malmaison, France.

ABSTRACT

In this paper, an improvement of the centrifuge method is presented. It consists of continuous determination of the local saturation, at three locations along a core, while centrifuging.

Usually, the centrifuge method only leads to a measure of fluid production, (i.e. average saturation) in a core at different rotation velocities. Then, the data are used to compute capillary pressure curves. But this transformation requires physical assumptions and mathematical procedures, which can generate large errors.

Our approach consists in (i) recording transit times of ultrasonic waves through three parts along the core, during the rotation, and, (ii) deducing local saturation by a specific and simple calibration. For oil-brine drainage in Vosges sandstone samples, the correspondence between transit times and saturation has been checked against CT Scanner analysis and imaging.

Using this approach, direct determinations (i.e. without any mathematical treatment) of capillary pressure curves are presented. These curves are in agreement with those obtained by the standard centrifuge method and by mercury injection. They are more accurate (higher number of measurements, Pc, S) or can be obtained more rapidly (for the same number of measurements) .

The main assumptions for the centrifuge method are evaluated. It is found that their failure is possible more often than usually reported.

To conclude our method leads to reliable local saturation measurements which are very useful for capillary pressure curve determination and for physical investigation of the centrifuge method as well.

INTRODUCTION

The centrifuge method is a powerful tool for the determination of capillary pressure and relative permeabilities versus the local saturation of fluids in core samples (Hassler and Brunner, 1945 ; Slobod et al., 1951 ; Hagoort, 1980; Firoozabadi et al., 1988, 1986). However this technique usually involves the measurement of the total fluid recovery only, leading to an average, and not local, saturation in the sample. The determination of the local saturation during centrifuging is thus related to a mathematical problem of inversion, itself related to assumptions on the local fluid distribution in the sample.

The mathematical problem, i.e., how to calculate the saturation profile or the capillary pressure curve from the production curve, has been extensively studied using simple, but approximate, analytical solutions or exact solutions usually related to complex and long numerical treatments (Hoffman, 1963 ; van Domselaar, 1964 ; Bentsen and Anli, 1977 ; Melrose, 1986 ; Rajan, 1986 ; Nortvedt and Kolltveit, 1988 ; Skuse et al, 1988 ; Ruth and Wong, 1988, 1990; Ayappa et al., 1989 ; Glotin et al., 1990 ; King et al., 1990 ; Hermansen et al., 1991 ; Jaimes, 1991). Forbes addressed this problem and proposed a new accurate, rapid and simple solution (Forbes, 1991).

The most important physical hypotheses concern the outflow boundary condition, continuity of fluid pathways, hydraulic equilibrium and absence of cavitation (O'Meara et al., 1988 ; Hirasaki et al., 1988) . Following Hassler and Brunner (1945), these assessments are used to evaluate the capillary pressure (Pc) along the core as a function of the rotation velocity. The boundary condition, i.e. 100% of wetting fluid saturation at the outlet core face, leads to Pc=0 at the outlet face (Fig. 1). The fluid continuity and hydraulic equilibrium give the pressure gradient in each phase, $dP/dr = \rho \omega^2 r$, where ρ is the phase density and ω the rotation velocity. Integrating in each phase along the radius r and subtracting the pressure of the non wetting phase to the pressure of the wetting phase : $Pc = \frac{(\rho_{wetting} - \rho_{non\text{-}wetting})}{2} \omega^2 (r^2 - r_{max}^2)$, at distance r from the centrifuge axe. Finally, this expression is used to calculate the capillary pressure curve from the cumulative fluid production.

The validity of both mathematical and physical assumptions can be investigated with the measurement of the saturation profile in the sample. This has been done by freezing one of the fluids while centrifuging and then measuring the saturation profile (O'Meara et al., 1988 ; Baardsen et al., 1989). Another method consists in using a colored epoxy resin as the wetting fluid, in solidifying the epoxy while centrifuging and finally in imaging and quantifying the fluid distribution from thin sections of the solidified sample (Wunderlich, 1985). Such methods lead to local saturation measurements but are time consuming and cannot be used with standard fluids.

A powerful improvement, which will preserve the quickness of the centrifuge method, is the measurement of the saturation profile during the centrifugation. Such an improvement has been proposed by Vinegar et al., 1987, based on an apparatus of X-ray imaging during centrifugation. However we do not know any published result from this technique. For the same purpose, we adapted an original, non time consuming technique, based on ultrasonic waves. Using this technique, we obtained local saturation values while centrifuging and used these values to calculate the capillary pressure curves and discuss the physical problems.

In a first part, we present (i) the ***experimental device***, (ii) the study of ultrasonic signal ***variations due to other causes than changes in fluid distribution***, (iii) a procedure to ***correct*** signals for these effects and finally (iiii) ***variations due to changes in fluid distribution***. In a second part, we propose (i) a ***rapid calibration*** method and (ii) the application to direct ***capillary pressure curve determination***. Finally, we show how the technique can be used (i) to discuss ***the centrifuge method*** and (ii) to develop ***further applications***.

EXPERIMENTAL BACKGROUND

The principle of the method is to emit an ultrasonic wave which passes through an oil-brine saturated core and to receive this wave on ceramic transducers (Bacri and Salin, 1986 ; Soucemarianadin et al., 1987 ; Hoyos et al., 1990 ; Aas et al., 1990 ; Lenormand et al., 1990 ; Bacri et al., 1991). The time between emission and reception in a given part of the core, transit time or time of flight, is measured and the corresponding fluid saturation is deduced. At the present time we measure ultrasonic transit time at 3 locations along centrifuged sample. The temperature in the centrifuge bowl is recorded (Fig. 1). The core is coated with a sleeve and is supported by 2 end-pieces which exactly fit the inner part of a holder. That allows an accurate positioning and repositioning of the core. The ultrasonic transducers are hold in 2 PTFE pieces which fit specific holes in the core holder. The whole device is placed in a common aluminium centrifuge core holder. Such a device reduced the volume allowed to be centrifuged to about 7 cm in length and 2.5 cm in diameter.

To calibrate the correspondence between ultrasonic signal and fluid saturation, we deduced saturation from CT scanner and gamma ray measurements. The accuracy of CT scanner analysis is given at +/- 2% for absolute error on saturation value. We compared the CT scanner oil saturation and the average oil saturation from our different drainage experiments (obtained by material balance from the measurement of the water production volume). The correspondence is satisfying and agrees to the accuracy of +/- 2 % in saturation. Conversely the statistical error of the gamma ray

technique is very large in our conditions (fluids are refined oil and synthetic brine without dopant) and we mainly operated by CT scanner analysis to investigate the relation of ultrasonic signal and fluid saturation.

In order to focus on the variation due to saturation changes only, we first studied how to prevent or correct those due to other causes.

VARIATIONS DUE TO OTHER CAUSES THAN CHANGES IN FLUID DISTRIBUTION

Temperature variations and rotation can affect the ultrasonic signals.

Effect of temperature variation

During each experiment the temperature variation is measured using a platinum gauge. The ultrasonic signal is obtained from transducers of the sample in the centrifuge core holder and from transducers of a reference sample, fixed in the centrifuge bowl (one phase saturated sample).

Correspondence between the relative transit time variation ($\Delta t/to$) and the temperature variation has been studied for Vosges sandstone samples (GV2, GV4, Table 1). The same trend has been obtained for small or large temperature variation as well, with a ratio $(\Delta t/to)/\Delta T$ of about 0.002 $°C^{-1}$ (in the range 25- 40°C). That is to say that a variation of +/- 2°C (usual accuracy in the centrifuge devices) induces a transit time variation of +/- 0.4 % which corresponds (see below) to an apparent absolute variation of +/- 8 % (or more) for the fluid saturations.

This demonstrates the need of a control and correction for temperature effect on ultrasonic measurement in a common centrifuge device. Figure 2 presents recordings of the temperature as controlled by the centrifuge, of transit time variations through the reference sample and of transit time variations through a rotating core (at 3 locations and for different rotation velocities, sample GV1). Oscillations are due to thermal regulation (20°C+/- 3°C) and large variations to saturation changes. It can be noted that the thermal equilibrium between the thermal gauge and the samples is not always obtained for such a centrifuge thermal control, while it is better between the reference and the rotating samples. Therefore a thermal correction can be made preferentially from the recording of the signal through the reference sample.

Effect of rotation

We assessed effect of rotation velocity in the centrifuge on the ultrasonic signal for a range of 0-3500 RPM which is the usual range for standard centrifuge (i.e. for Pc from 1 to about 13 bars). We centrifuged a sample, (GV4 Vosges sandstone, Table 1) at different speeds (0 to 3500 RPM). This sample was saturated with the oil contained in the core holder. Therefore no saturation variation was possible (Soil = Const.=100%). The correction for temperature

variation effect was made with the recording from the reference sample and the GV4 sample was not removed from the core holder during the experiment. In such a case, the resulting ultrasonic signal is expected to represent the effect of rotation only. That effect appears to be small. The induced ($\Delta t/to$) value is lower than +/- 0.0005 between 0 and 2000 RPM and increases to +/- 0.002 between 2000 and 3500 RPM. In the experiments described below the same effects can be obtained for absolute saturation changes of +/- 1% and +/- 4 % respectively.

Signal Correction

At that point, we noted that the thermal correction is the main correction to be taken into account. However it is possible to simply obtain a global correction (thermal, pressure, electrical effects.....) from the recording of one of the signals from the rotating sample itself. This gives the more accurate correction. It consists in using the ultrasonic signal measured in a part of the rotating sample , where the saturation is known to be constant.

For instance, during the early stage of drainage experiments, the water saturation remains constant (100%) in the outlet part of the sample, while, during the late drainage stage it is constant (Swi) in the inlet part of the sample.

Signal variation in these parts are due to other effects than saturation change and have been successfully subtracted to correct signals from other parts. This is illustrated on Figure 2. Recordings from the middle (No.2) or the bottom (No.1) can be used as references for correction until 830 RPM and 865 RPM respectively.

VARIATIONS DUE TO CHANGES IN FLUID DISTRIBUTION

Method of measurement

The relative transit time variation is measured during centrifuging, then the centrifuge is stopped and another, static, method (CT Scan mainly) is used to measure the corresponding saturation. To validate such an approach we had to show that saturation changes are small during the time between the two measurements which therefore closely correspond to the same sample state.

Firstly we studied the possibility of such saturation changes by recording the ultrasonic signal when the centrifuge is stopped and after (Fig. 3). For an early drainage stage, Figure 3a presents the relative transit time variation ($\Delta t/to$) in a Vosges sandstone sample (GV4) which has been centrifuged at different velocity steps, 700, 750 and 850 RPM, and kept static (0 RPM) after the two last steps. It can be seen that the signal varies just when the centrifuge is stopped or started. However, there is no significant variation during the static period even over several hours (Fig. 3a). For an advanced drainage stage, Figure 3b shows the signal variation after the sample GV1 has been rotated at 1000 RPM and then stopped. Again, only slight variation are recorded over more than one hour. Conversely, for a late

drainage stage (1500 RPM, Figure 3b) we observe a rapid change in the signal for the lower point of measurement (sample bottom). It can also be noted that this change is partly preserved when the sample is rotated again at the same velocity (1500 RPM, Figure 3b).

Secondly, to confirm and quantify these observations in terms of oil saturation, the experiment has been reproduced by centrifuging samples at different velocity steps, stopping the centrifuge, measuring and imaging the saturation distribution in these samples over one hour or more after each velocity step. CT scanner or Gamma Ray attenuation techniques have been used for Vosges sandstone and Berea sandstone samples respectively. Figure 4 shows the saturation evolution, versus time, after two steps of rotation speed (GV6 sample, Table 1). The saturation values are the average values for each slice of core in front of the 3 couples of ultrasonic transducer (see Figure 1). The same observations than those previously done with the ultrasonic recording can be made :

-for early or advanced drainage stages the saturation variations are small except for long time (24 hours, Fig. 4a),

-for a late drainage state significant variations specifically occur in the bottom of the sample (Fig. 4b).

In Figure 4c, we present saturation profiles at the beginning of a CT scanner analysis after the 800 RPM and 1020 RPM steps and, at 3 different moments during the CT scanner analysis after the 1500 RPM step. It is noted that the oil-water front is sharper at advanced and late drainage stages. This induces higher saturation gradient and then higher disequilibrium as soon as the rotation is stopped. It could explain the more rapid variation of saturation in the front zone of the late stage, i.e. in the bottom of the sample (No.1) after the 1500 RPM step. The 100% water saturation zone does not exist at sample end face , 6 minutes and 20 seconds after the centrifuge was run at 1500 RPM and stopped, (boundary condition, Fig. 4c). However we cannot know whether that face was fully water saturated or not while centrifuging. Changes in fluid saturation can be due to redistribution during deceleration or after. The oil phase could imbibe from the outlet face in the case of a thin water film at that face.

To conclude, our successive measurements of the ultrasonic signal and saturation can be related to very similar sample states, excepted in a late drainage stage for the measurements in the sample outlet part (bottom). In this last case, the oil saturation could be significantly over-estimated, otherwise small variations only are observed during the first 5 minutes after the centrifuge was stopped. Such effects have to be minimized by making the time between the centrifuge stop and the saturation measurements as short as possible. In our study we measured the saturation, using the CT scanner device, between 2 and 6 minutes after the centrifuge stop.

Variation of transit time due to changes in saturation

In order to obtain "transit time versus saturation" relationships we performed several experiments at different velocity steps. The experiments consist of drainage on different Vosges sandstone core samples of 2.5 cm in diameter, about 7 cm in length, 23 % porosity and 500-600 mD for air permeability (Table 1). That sandstone is known to be homogeneous with some spots of iron-oxydes cement. Fluids are brine (50g/l NaCl) and refined oil (mixture of Albelf and Soltrol 130) with 15 cp viscosity at 20°C. Interfacial tension is 40 mN/m at 20°C (Table 1). In the centrifuge core holder, the end face of the sample (r_{max}) is at 15.6 cm from the rotation axis. Transducers (ultrasonic measurements) are located at 50, 29 and 8 mm from the end face to the axis and labelled by top, middle and bottom respectively (Fig. 1).

The duration of each velocity step is chosen in order to obtain an apparent equilibrium, i.e. we decide to stop the centrifuge when the water production volume and the ultrasonic signals seem to be constant. After stopping the centrifuge and the signal recording, the inner core holder ,with the sample, is removed and the total fluid production is measured. The local fluid saturation is then measured using CT Scanner analysis at the locations of the transducers which are used to measure the ultrasonic signal. In order to check the consistency of measurements, the average saturation is also measured and compared to the total fluid production.

The inner core holder is then replaced in the centrifuge and is run again at the previous velocity while the recording is restarted. Then the rotation speed is increased to the next step and the same procedure is applied.

Finally, for each location along the sample, we plotted the CT scanner saturation as a function of transit time variation at apparent equilibrium for the different velocity steps.

Figure 5a gives an example of recording of the relative transit time variation ($\Delta t/to$) versus time for the 3 locations along core samples during centrifuging. Vertical dashed lines indicate changes in rotation velocity step. Blanks between the lines represent the stop for CT scanner measurements of saturation. The relative transit time variation has been corrected as previously mentioned (see "signal correction"). Figures 5b, 6 and 7 are the plots of CT scanner oil saturation values against values of corresponding relative transit time variation for different experiments and different velocity steps.

The following comments can be made :

- (i) the ultrasonic recordings are as expected, i.e. they show that the water-oil front goes from the inlet face to the end face of the core, from top (No.3) to bottom (No.1) couples of transducers.

• (ii) when the rotation speed increases, relative transit time variations for the 2 upper locations increase approximately to the same plateau value. This corresponds to a uniform irreducible water saturation and a homogeneous effect of the saturation on ultrasonic signals.

• (iii) the plots "oil saturation / relative transit time variation" show quasi-linear behaviors until the residual water saturation is reached. According to error due to correction (thermal, rotation, pressure.... effects), to possible changes in the fluid distribution before CT scanner analysis and to the possible problem of repositionning, a linear behavior seems to be the most simple and realistic conclusion at the present time.

• (iv) from a location to another, in a given sample, and from a sample to another, the calibration lines are close and about : $S_o = a\ (\Delta t/to)$, with a= 19 to 23 (GV1 to GV6 Vosges sandstone samples for drainage experiments in our device).

• (v) when the residual water saturation is reached or almost reached, variation of saturation is expected to be small but significant variation of ultrasonic signals can be observed (no more or low water production) (Fig. 5a, 3000 RPM ; Fig. 8d, 2200 to 3500 RPM). That is unexpected under the assumptions for the centrifuge method. It is noted that such variations occur first in the outlet part of the core (bottom, No.1), then in the middle and finally in the inlet part of the core (top, No.3) (Fig. 8d). The signal values are in reverted order with higher signals from the bottom (No.1) and lower signals from the top (No.3) parts of the core. On the "oil saturation / relative transit time variation" curves, it leads to a more or less flat part (Fig. 11b to 13b) which is not relevant for the drainage experiment under effective Hassler and Brunner assumptions.

The (iii) and (iv) observations can be retained in order to obtain a very rapid calibration procedure for any drainage experiment. We now assume that the linear correspondence between oil saturation and "relative transit time variation" may be a good approximate behavior. Similar linear behavior is supported by data from Bacri and Salin (1986) or Bacri et al. (1991) for displacement drainage in sandstone saturated with oil and brine.

RAPID CALIBRATION

Assuming a linear relationship between oil saturation and "relative transit time variation", we only need one point $\{S_o ; \Delta t/to\}$, in addition to the point $\{0 ; 0\}$, to obtain the correspondence between S_o and $(\Delta t/to)$. This single point can be obtained easily for homogeneous sample as follows :

When centrifuging a homogeneous sample, at a high enough rotation speed, the saturation becomes close to the irreducible water saturation in a large part of the sample. The common measurement of the total water production leads to the average saturation which is therefore close to the local saturation value.

The measurement of the plateau value for ultrasonic transit time variation (constant value for different rotation velocities) gives the corresponding $\Delta t/to$ value.

For instance, when running the Vosges sandstone GV1 at 3000 RPM (Fig. 3b) we obtained a water production which corresponds to 71.4 % for the average oil saturation and measured for the plateau value $(\Delta t/to) \approx 0.0325$. That is to say $S_o \approx 22\ (\Delta t/to)$ as obtained previously from a much longer procedure (CT Scanner measurements).

We also note that it is not necessary to centrifuge at high rotation speed to obtain the $(\Delta t/to)$ which corresponds to irreducible water saturation, because this plateau value is obtained for low speed in the inlet part of the sample. In the case of the Berea sandstone sample BA1 (Table 1, residual water saturation = 34.7%) we observed a plateau at $(\Delta t/to) = 0.0178$ for velocities higher than 1200 RPM on the measurement at sample top and a plateau at $(\Delta t/to) = 0.0175$ for a velocity higher than 1620 RPM in the middle of the sample. This directly leads to $S_o \approx 37$ $(\Delta t/to)$ (Berea sandstone in our device). The linear correspondence between oil saturation and "relative transit time variation" is an hypothesis which has been herein only evidenced for Vosges sandstone samples. However this hypothesis also leads to realistic results for Berea sandstone (see below).

CAPILLARY PRESSURE CURVE DETERMINATION

To obtain a capillary pressure curve we first applied the current method. The sample is run at different velocity steps and, at each step, an apparent equilibrium is waited for. The inlet face capillary pressure and the average saturation are obtained (by measuring the water volume production). The data {inlet face capillary pressure - average saturation} are then used to reconstruct the capillary pressure curve (Forbes, 1991).

In the present case we recorded in addition the transit time variation at the locations of the transducer couples. The local oil saturation values are obtained directly from the transit time step values. The corresponding capillary pressure values are calculated at the same location, exactly as the inlet capillary pressure in the classical method, i.e. assuming fluid equilibrium, the boundary condition and the continuity of fluid pathways (Pc=0 at end face; $Pc = \frac{(\rho_{water} - \rho_{oil})}{2} \omega^2 (r^2 - r_{max}^2)$ at distance r from the axis).

The recording allows also

-to check if the fluid equilibrium is actually near to be reached or not (plateau shape on the steps of ultrasonic recording) when the water production has apparently stopped and,

-to partly check the boundary condition (the boundary condition S_{oil}=0, Pc=0 at end face is certainly verified when S_o=0 at the lower location of recording, No.1).

The capillary pressure curves have also been independently obtained on twin samples from the classical mercury injection method. Then, the current scaling procedure (Leverett, 1941) has been applied for comparison to those obtained from the centrifuge. That has been done for the Vosges sandstone sample GV3 (Figures 8, 9 and Table 2). The capillary pressure curve obtained by the standard interpretation of centrifuge data (dashed line, Fig. 9) , the curve obtained by mercury injection (Fig. 9) and the capillary pressure / saturation values directly obtained from ultrasonic device are in agreement. The boundary condition is effective up to, at least, 1220 RPM (Fig. 8b). Figures10 and Table 3 show results of an experiment performed on the Vosges sandstone sample GV1. The same good agreement between the different methods used to obtain capillary pressure curves is noticed, except for one curve (bottom recording, No.1). That has also been done for a Berea sandstone sample (Table 4, Fig. 11). The capillary pressure curve obtained by the standard interpretation of centrifuge data (dashed line, Fig. 11) and the capillary pressure / saturation values directly obtained from ultrasonic device are again in agreement.

It is concluded that ultrasonic measurement and assumption of a linear relationship with saturation lead to relevant saturation measurements and that capillary pressure curves can be obtained more accurately (higher number of measurements) or more rapidly (lower number of velocity steps) than in the conventional method.

DISCUSSION ON THE CENTRIFUGE METHOD

Cavitation.

Ultrasonic measurements are very sensitive to gas occurrence and have been successfully used to detect gas bubbles (Hoyos et al., 1991). They can be considered as an efficient tool to evidence cavitation. In our experiments, regular variation of signals indicate that no cavitation occurred. Theoretically, cavitation is expected to mainly occur in gas-liquid system (Hirasaki et al. 1988). We confirm herein, that it is not the main limitation when centrifuging a liquid-liquid system in core sample.

Equilibrium time

As previously said the continuous recording of the ultrasonic signal allows to adapt the duration of a rotation velocity step in oder to wait for an "apparent" hydraulic equilibrium. "Apparent" means that, over one to few hours, local saturation values seem constant at the different locations of recording. Of course, actual equilibrium is not exactly reached and measured signal values could be few percent lower that the true equilibrium values. This could finally lead to errors of the same magnitude in the capillary pressure curve because we construct the curve directly from the local measurements.

In the standard centrifuge method, when only the cumulative fluid recovery is recorded, we have to use a mathematical or / and numerical treatment to reconstruct the capillary pressure curve (calculation of inlet face saturation). That reconstruction is known to be ill-conditioned (Forbes, 1991 ; Hermansen et al., 1991; Ayappa et al., 1989; Linz, 1969, 1982). It increases considerably the uncertainties of recovery values which lead to large errors in the capillary pressure curve. That explains that in the standard centrifuge method errors due to the failure of hydraulic equilibrium could be important and that some authors have proposed methods to assess the equilibrium recovery value from the recording of non equilibrium data (O'Meara et al., 1988 ; King et al., 1990).

In the present case, we directly obtain the local saturation values, no ill-conditioned procedure has to be used and uncertainties are not enlarged. When the occurrence of equilibrium is checked by local recordings, we believe that saturation values are very close to the true equilibrium values. Consequently, the 'equilibrium time' limitation is not of prime importance in our device, providing it is checked from ultrasonic recording shapes.

Boundary and continuity of fluid pathways conditions.

As previously mentioned significant variations of ultrasonic signals can be observed at the end of experiments while no, or low, water production is observed (Fig. 11a, 12a, 14d). As far as these variations propagate from the oulet to inlet face of the core, changes in the local fluid distribution occur, firstly and strongly at the end face of the sample. It indicates that the capillary pressure regime changes (oil breakthrough, failure of the boundary condition for instance) or that the capillary pressure concept vanishes (failure of the fluid phase continuity). In both cases the conditions for assuming the capillary pressure is $Pc=\frac{(\rho_{water}-\rho_{oil})}{2}\omega^2 (r^2 - r_{max}^2)$, are no more effective and the centrifuge method fails.

For sample GV3 (Figures 8, 9 and Table 2), the conditions are no more effective above 2200 RPM when inverted signals are evidenced (Fig. 8d). In the case of sample GV1, however, the failure has not been clearly evidenced

while the ultrasonic recordings from the different locations do not lead to the same final plateau values. It occurs at, or below, 1840 RPM as far as we observe a continuous increase but no more jump in the signal when increasing the velocity to higher values. That could explain that capillary pressure curve constructed for the bottom location (No.1) does not correspond to other curves because it mainly involves measurements at high velocity (after the possible failure of Hassler and Brunner conditions, Fig. 10).

From these experiments, it is noted that the failure of the conditions could occur for rotation speed of about 1800-2200 RPM. This corresponds to inlet face capillary pressure of about 650-1000 mbar . This value is significantly lower than values usually considered for the failure of the boundary condition (4 to more than 10 bar ; Wunderlich, 1985 ; Melrose, 1988). The failure of the centrifuge method is therefore possible in very common conditions although it is reported that the failure of the boundary condition occurs only in unusual circumstances (Melrose, 1988 ; O'Meara et al., 1988 ; Donaldson et al., 1991).

Baardsen et al. (1991) also reported the loss of the 100% water saturation at quite low pressure, by CT scanner imaging of centrifuged samples, but this loss was not clearly related to the failure of the boundary condition or to some fluid redistribution during deceleration (exactly as in our Figure 10).

Finally, for the use of centrifuge method in a liquid-liquid system, the boundary condition or continuity of fluid pathways (used to calculate the capillary pressure along core) appear to be the conditions which could fail the more easily. They are of prime importance by comparison with other assumptions as absence of cavitation or effective hydraulic equilibrium. They have to be carefully checked. At the moment the best way is probably to compare, using the same experiment, capillary pressure curves as obtained from local saturation measurements and as reconstructed with production data according to usual centrifuge method (Fig. 9, 10, 11). If these curves are in agreement, either the different assumptions for use of the centrifuge method are effective, or , if they fail, the failure is not significant enough to largely change the results.

This emphasizes the advantage of this easy and rapid method to determine if the physical assumptions of the centrifuge method are valid or not.

FURTHER APPLICATIONS

To obtain the capillary pressure curve, we used ultrasonic signals to deduce saturation distribution at (or near) equilibrium for different rotation velocities. The variation, versus time, of signals at a given location along the core is

used only to check the effectiveness of equilibrium. However, this device is much more informative as it leads also to local saturation changes in transient regimes (unsteady states), which highly depend on relative permeability values.

In the near future, transient variations of saturation (and pressure), along the core, will be simulated using a one-dimensional, two-phase incompressible and immiscible model based on Darcy's law (Chardaire-Rivière et al., in prep.). The next step will be to couple this resolution to an adjustment procedure to obtain simultaneously the relative permeability and capillary pressure curves (Chardaire et al., 1989, 1990). Recently, numerous methods to estimate relative permeability curves from centrifuge or displacement measurements have been proposed (O'Meara and Crump, 1985 ; Nordtvett et al., 1990 ; Chardaire et al., 1989, 1990 ; King et al., 1990 ; Munkvold and Torsaeter, 1990 ; Grattoni and Bidner, 1990). Such a development is linked to a lot of new procedures, history matching schemes, for estimating relative permeability and is also linked to some new measurement techniques which allow the collection of non equilibrium production data while centrifuging (O'Meara and Lease, 1983 ; Munkvold and Torsaeter, 1990). The fact is that the limitation arises in the way to obtain relevant data and not in the way of their interpretation in terms of relative permeability. At the moment most of the interpretations are made from production data only, i.e. only from cumulative global fluid recovery or flow rate measurements. It could lead to insufficient constraints for the relative permeability determination whatever the accuracy of the interpretation procedure. For instance, Firoozabadi and Aziz (1986) have demonstrated that actual recoveries could be closely matched with several and very different sets of relative permeability curves.

From that point of view, our method, leading to local saturation variation values during transient regimes and in several locations along the sample, will highly increase the quality (local rather than average) and the number of data to be matched. Singleness of interpretation in terms of relative permeability is actually expected from such kind of data.

CONCLUSION

A technical device and procedure for ultrasonic measurements while centrifuging which operates with 3 locations of measurement along core samples has been designed.

From local saturations measured by CT scanner analysis, the type of relationship between ultrasonic signal and saturation has been studied for drainage on Vosges sandstone samples with refined oil and synthetic brine. A linear relationship is proposed and a simplified procedure of calibration (without CT scanner measurement) is described.

Applying that procedure and ultrasonic measurements, relevant capillary pressure curves have been obtained for both Vosges and Berea sandstone samples with refined oil and brine. Presently, the method appears to be

reliable to measure local saturation while centrifuging at least for drainage experiments on sandstone, with refined oil and brine, and in the range 0-3500 RPM for the rotation velocity.

It has been also used qualitatively to evidence any change, or absence of change, in fluid distribution while centrifuging and therefore to study physical assumptions for the centrifuge method. Usual hypotheses, as boundary or continuity of fluid pathways, are found to be the main hypotheses by comparison with other usual assumptions (cavitation, hydraulic equilibrium). The failure of such hypotheses is shown to be possible in more common circumstances than usually reported.

Further applications of our method will consist in the determination of relative permeability curves by numerical matching of local saturation recordings during transient regimes while centrifuging. The method is expected to increase the quality and the number of data to be matched and therefore to significantly increase the accuracy of relative permeability curve determination.

NOMENCLATURE

Latin	r	Radial distance from the centrifuge axis to a point in the centrifuged core
	r_{min}	r at the inner core face
	r_{max}	r at the outer core face
	Pc	Capillary pressure
	S	Phase saturation
	S_w	Water saturation
	S_o	Oil saturation
	t	Transit time (or time of flight) of ultrasonic waves
	t_o	Initial transit time
	T	Temperature
	℃	Celsius degree
	RPM	Rotation per minute
Greek	ρ	Phase density
	Δt	Difference between transit time values
	ΔT	Difference between temperature values
	ω	Centrifuge angular velocity
	σ	Interfacial tension
	θ	Contact angle
Subscripts		
	o	Refers to oil
	w	Refers to water
	wetting	Refers to wetting phase
	non-wetting	Refers to non-wetting phase
	mercury	Refers to mercury
	vapor	Refers to mercury vapor
	max	Refers to the outer core face
	c	Capillary
	o	Refers to initial value

AKNOWLEDGEMENTS

This study is a part of a work funded by AMOCO, JNOC, MOBIL, NORSK HYDRO, SAGA, SNEAP, STATOIL, TOTAL and IFP. We thank these companies for their support.

REFERENCES

Aas M., Bacri J-C, Frénois C., Salin D. and Wouméni R., 1990 , 3-D acoustic scanner : 65 th Conference of the SPE, New Orleans, Louisiana, USA, SPE 20599.

Ayappa K.G., Davis H.T., Davis E.A. et Gordon J., 1989, Capillary Pressure, Centrifuge Method Revisited : AIChE Journal, V. 35, No. 3, p. 365-372.

Baardsen H., Nilsen V., Leknes J. and Hove A., 1989 , Quantifying Saturation Distribution and Capillary Pressures Using Centrifuge and Computer Tomography : NIPER / DOE, June 1989, 20 p.

Bacri J.C. and Salin D., 1986 : Sound Velocity of a Sandstone Saturated with Oil and Brine at Different Concentrations : Geophysical Research Letters, V. 13, 4, p. 326-328.

Bacri J.C., Hoyos M., Rakotomalala N., Salin D., Bourlion M., Daccord G., Lenormand R. and Soucemarianadin S, 1991, Ultrasonic Diagnostic in Porous Media and Suspensions : J. Phys., France, III, 1, p. 1455 - 1466.

Bentsen R.G. and Anli J., 1977, Using Parameter Estimation Techniques to Convert Centrifuge Data into Capillary Pressure Curve : SPE Journal, p. 57-64.

Chardaire-Rivière C., Chavent G., Jaffre J., Liu J., and Bourbiaux B., 1989, Simultaneous Estimation of Relative Permeabilities and Capillary Pressure : 64 th SPE Annual Technical Conference and Exhibition, San Antonio, USA, SPE 19680, p. 499 - 506.

Chardaire C., Chavent G., Jaffre J. and Liu J., 1990, Multiscale Estimation of Relative Permeabilities and Capillary Pressure : 65 th SPE Annual Technical Conference and Exhibition, New Orleans, Louisiana, USA, SPE 20501, p. 303 - 312.

Chardaire-Rivière C., Forbes P., Chavent G., Zhang J., Deflandre Fand Lenormand R., in preparation, Improvement of Centrifuge Technique by Measuring Local Saturation : 1992 SPE Annual Technical Conference and Exhibition, Washigton , USA, October 4-7, SPE 24882.

van Domselaar H.R., 1964, An Exact Equation to Calculate Actual Saturations from Centrifuge Capillary Pressure Measurements : Rev. Tec. INTEVEP, V. 4, N. 1, p. 55-62.

Donaldson E.C., Ewall N. and Singh B., 1991, Characteristics of Capillary Pressure Curves : Journal of Petroleum Science and Engineering, 6, p. 249 - 261.

Firoozabadi A. and Aziz K., 1986, Relative Permeability from Centrifuge Data. SPE paper 15059. 56th 'California Regional Meeting/Oakland', p. 127-139.

Firoozabadi A., Soroosh H. and Honarpour G., 1988, Drainage Performance and Capillary Pressure Curves with a New Centrifuge : J. Petr. Tech., p. 45-64.

Forbes P.L., 1991, Simple and Accurate Methods for Converting Centrifuge Data into Drainage and Imbibition Capillary Pressure Curves : 1991 Society of core analysts annual technical conference, August 20-22, San Antonio, paper 9107, 15 p.

Glotin J. Genet J. and Klein P., 1990, Computation of Drainage and Imbibition Capillary Pressure Curves from Centrifuge Experiments. SPE paper 20502 : 1990 Annual Technical Conference and Exhibition, New Orleans, Sept. 23-26, p. 313-324.

Grattoni C.A. and Bidner M.S., 1990, History Matching of Unsteady - State Corefloods for Determining Capillary Pressure and Relative Permeability. SPE paper 21135, SPE Latin American Petroleum Engineering Conference, Rio de Janeiro, October 14 - 19, 8 p.

Hagoort J., 1980, Oil Recovery by Gravity Drainage : SPE Journal, p. 139-150.

Hassler G.L. et Brunner E., 1945, Measurements of Capillary Pressure in Small Core Samples : Trans. AIME, 160, p. 114-123.

Hermansen H., Eliassen O., Guo Y. and Skjaeveland S.M., 1991, Capillary Pressure from Centrifuge- A New Direct Method : 1991 SCA Conference Eurocas, London.

Hirasaki G.J. , O'Meara D.J. and Rohan J.A., 1988, Centrifuge Measurements of Capillary Pressure, Part 2 - Cavitation, SPE paper 18592, SPE Annual Technical Conference and Exhibition, Houston, Texas, USA, 13 p.

Hoffman R.N., 1963, A Technique for the Determination of Capillary Pressure Curves Using a Constantly Accelerated centrifuge : Trans AIME, 228, p. 227-235.

Hoyos M., Moulu J.C., Deflandre F. and Lenormand R., 1990, Ultrasonic Measurement of the Bubble Nucleation Rate during Depletion Experiments in a Rock Sample : 65 th SPE Annual Technical Conference and Exhibition, New Orleans, Louisiana, USA, SPE 20525.

Jaimes O., 1991, Centrifuge Capillary Pressure : Method of the Center of Forces. SPE paper 22687, Annual Technical Conference and Exhibition, Dallas, October 6 - 9, p. 293 - 303.

King M.J., Narayanan K.R. and Falzone A.J., 1990, Advances in Centrifuge Methodology for Core Analysis : 1990 SCA Conference, Paper 9011, 24 p. .

Lenormand R., Forbes P., Hoyos M. and Deflandre F., 1990, Mesure de la Répartition des Concentrations de Constituants d'un Système en Centrifugation par Emission / Réception de Signaux Mécaniques. Patent filed, September 1990.

Leverett M. C., 1941, Capillary Behavior in Porous Solids : Trans. AIME, No. 142, p. 152 - 168.

Linz P., 1969, Numerical Method for Volterra Integral Equations of the First kind : Comp. Journal, 12, 393-397

Linz P., 1982, The Solution of Volterra Equations of the First Kind in the presence of large incertainties : Treatment of Intergral Equations by Numerical Methods, 123, Baker C.T.H. and Miller G.F. eds.

Melrose J.C., 1986, Interpretation of Centrifuge Capillary Pressure Data : SPWLA Annual Logging Symp., June 9-13, p. 1-21.

Melrose J.C., 1988, Interpretation of Centrifuge Capillary Pressure data : The Log Analyst, p. 40 - 47.

Munkvold F.R. and Torsaeter O., 1990, Relative Permeability from Centrifuge and Unsteady State Experiments. SPE paper 21103 : SPE Latin American Petroleum Engineering Conference, Rio de Janeiro, October 14 - 19, 13 p.

.

Nordtvedt, J.E. and Kolltveit K., 1988, Capillary Pressure Curve from Centrifuge Data by Use of Spline Functions, SPE unsolicited paper 19019 .

Nordtvedt, J.E. , Watson A.T., Mejia G. and Yang P., 1990, Estimation of Capillary Pressure and Relative Permeability Functions From Centrifuge Experiments. SPE unsolicited paper 20805.

O'Meara D.J. and Lease W.D.,1983, Multiphase Relative Permeability Measurements Using an Automated Centrifuge. SPE paper 12128 : 58 th Annual Technical Conference and Exhibition, San Francisco, October. 5 - 8.

O'Meara D.J. and Crump J.G., 1985, Measuring Capillary Pressure and Relative Permeability in a Single Centrifuge Experiment. SPE paper 14419 : 60 th Annual Technical Conference and Exhibition, Las Vegas, Sept. 22-25, 14. p. .

O'Meara D.J., Hirasaki G.J. and Rohan J.A., 1988, Centrifuge Measurements of Capillary Pressure, Part 1-Outflow Boundary Condition. SPE paper 18296 : Annual Technical Conference Houston, Texas, USA.

Rajan, R.R., 1986, Theoretically Correct Analytical Solution for Calculating Capillary Pressure-Saturation from Centifuge experiments : SPWLA Annual Logging Symp., June 9-13, p. 1-17.

Ruth D., and Wong S., 1988, Calculation of Capillary Pressure Curves from Data Obtained by the Centrifuge Method : 1988 SCA Conference, Aug 17-18, paper 8802, 9 p.

Ruth D., and Wong S., 1990, Centrifuge Capillary Pressure Curves : Journal of Canadian Petroleum Technology, v. 29, N. 3, p. 67-72.

Skuse B., Firoozabadi A.. and Ramey H.J., 1988, Computation and Interpretation of Capillary Pressure from a Centrifuge. SPE paper 18297 : Annual Technical Conference,Houston, Octb. 2-5, p..

Slobod R.L., Chambers A. and Prehn W.L., 1951, Use of Centrifuge For Determining Connate Water, Residual Oil, and Capillary Pressure Curves of Small Core Samples : Pet. Transac. AIME, v. 192, p. 127-134.

Soucemarianadin A., Bourlion M. et Lenormand R., 1987, Ultrasonic saturation mapping in porous media. SPE paper 16953 : Annual Fall Technical Conference and Exhibition, Dallas, 27-30 Septembre 1987. S. 205-212.

Vinegar H.J., O'Meara D.J. and Rohan A., 1987, Method and Apparatus for Determining Distribution of Fluids : United States Patent, 4 671 102, June 1987.

Wunderlich R.W., 1985, Imaging of Wetting and Non-wetting Phase Distribution - Application to Centrifuge Capillary Pressure Measurements, SPE paper 14422 : 60 th Annual Technical Conference and Exhibition, Las Vegas, Sept. 22-25, 12. p. .

TABLE 1 : CORE SAMPLES AND FLUIDS CHARACTERISTICS

CORE SAMPLES

Vosges sandstone	diameter mm	Length mm	porosity %	K_{air} md
GV1	25	69.5	23.6	618
GV2	25	69.5	24.7	--
GV3	25	71.0	23.4	513
GV4	25	---	---	
GV5	25	69.5	24.0	--
GV6	25	69.5	23.9	--

Berea sandstone	diameter mm	Length mm	porosity %	K_{air} md
BA1	25	73.5	19.0	143

FLUIDS

	density (g/cc)	viscosity (cp)	superficial tension (mN/m)	
temperature (°C)	20	20	20	30
Oil (Albelf+Soltrol)	0.822	15	26.7	25.5
Brine (50g/l NaCl)	1.036	--	70.2	--
Mercury			480	(cos θ =-0.76)

Interfacial tension $\sigma_{oil/water}$: 40 mN/m (20°C)

35 mN/m (30°C)

Corrective factor for mercury injection capillary pressure curves (20°C):

$$\frac{\sigma_{oil/water}}{\sigma_{mercury/vapor}\cos\theta} = \frac{40}{480 \times 0.76} = 0.1097$$

TABLE 2 : VOSGES SANDSTONE GV3 - DRAINAGE CAPILLARY PRESSURE CURVES

VOSGES GV3 pore volume 8.3 cc

irreducible water saturation 0.253

RPM	water prod. volume (cc)	Pc at inlet face (mbar)	average water saturation	Pc curve by usual method: Pc (mbar)	Pc curve by usual method: S water	Pc curve from ultrasonic measurements: location N°3 (top) Pc (mbar)	location N°3 (top) S water	location N°2 (middle) Pc (mbar)	location N°2 (middle) S water	location N°1 (bottom) Pc (mbar)	location N°1 (bottom) S water
455	0	41.151	1.000	41.151	1.000	31.823	1.000	19.936	1.000	5.908	1.000
515	0.2	52.719	0.976	48.948	0.950	40.769	1.000	25.541	1.000	7.569	1.000
560	0.3	62.335	0.964	59.200	0.906	48.205	1.000	30.200	1.000	8.949	1.000
590	0.5	69.192	0.940	66.957	0.784	53.508	1.000	33.522	1.000	9.934	1.000
635	0.7	80.150	0.916	76.578	0.600	61.981	0.996	38.830	1.000	11.507	1.000
680	1.4	91.912	0.831	88.078	0.463	71.077	0.719	44.529	1.000	13.195	1.000
740	2.1	108.847	0.747	103.327	0.370	84.174	0.470	52.734	1.000	15.627	1.000
780	2.7	120.933	0.675	116.993	0.300	93.519	0.398	58.589	0.967	17.362	1.000
840	3	140.253	0.639	133.955	0.270	108.460	0.345	67.949	0.771	20.136	1.000
900	3.2	161.005	0.614	154.240	0.260	124.508	0.310	78.003	0.502	23.115	1.000
940	3.5	175.635	0.578	170.866	0.260	135.821	0.297	85.091	0.401	25.215	1.000
995	3.8	196.789	0.542	189.893	0.260	152.180	0.285	95.339	0.344	28.252	1.000
1020	4	206.802	0.518	203.538	0.260	159.924	0.278	100.190	0.322	29.690	1.000
1090	4.4	236.161	0.470	226.590	0.260	182.627	0.259	114.414	0.285	33.905	1.000
1160	4.4	267.467	0.470	257.262	0.260	206.837	0.253	129.581	0.262	38.399	1.000
1220	4.5	295.852	0.458	286.599	0.260	228.787	0.253	143.333	0.253	42.474	1.000
1280	5	325.667	0.398	315.948	0.260	251.844	0.253	157.778	0.253	46.755	0.943
1330	5.1	351.607	0.386	343.151	0.260	271.904	0.253	170.345	0.253	50.479	0.909
1380	5.2	378.541	0.373	369.761	0.260	292.732	0.253	183.393	0.253	54.345	0.861
1460	5.3	423.702	0.361	408.980	0.260	327.656	0.253	205.273	0.253	60.829	0.779
1540	5.4	471.407	0.349	455.856	0.260	364.547	0.253	228.385	0.253	67.678	0.701
1700	5.5	574.450	0.337	540.860	0.260	444.232	0.253	278.306	0.253	82.471	0.549
1900	5.6	717.566	0.325	670.913	0.260	554.906	0.253	347.642	0.253	103.018	0.401

TABLE 2

TABLE 3 : VOSGES SANDSTONE GV1 - DRAINAGE CAPILLARY PRESSURE CURVES

VOSGES GV1 pore volume 8.27 cc

irreducible water saturation 0.202

PPM	water prod. volume (cc)	Pc at inlet face (mbar)	average water saturation	Pc curve by usual method: Pc (mbar)	Pc curve by usual method: S water	Pc curve from ultrasonic measurements: location N°3 (top) Pc (mbar)	location N°3 (top) S water	location N°2 (middle) Pc (mbar)	location N°2 (middle) S water	location N°1 (bottom) Pc (mbar)	location N°1 (bottom) S water
390	0	30.08	1.000	31.64	1.000	23.38	1.000	14.65	1.000	4.34	1.000
445	0.1	39.16	0.988	37.90	1.000	30.44	1.000	19.07	1.000	5.65	1.000
485	0.2	46.52	0.976	46.00	1.000	36.16	1.000	22.65	1.000	6.71	1.000
525	0.25	54.51	0.970	53.94	0.970	42.37	1.000	26.54	1.000	7.87	1.000
600	0.3	71.19	0.964	68.04	0.900	55.34	0.968	34.67	1.000	10.27	1.000
690	1.2	94.15	0.855	89.28	0.450	73.18	0.806	45.85	1.000	13.59	1.000
740	1.9	108.29	0.770	106.55	0.380	84.17	0.457	52.73	1.000	15.63	1.000
790	2.3	123.42	0.722	121.56	0.320	95.93	0.363	60.10	1.000	17.81	1.000
830	2.6	136.24	0.686	135.30	0.300	105.89	0.325	66.34	0.991	19.66	1.000
865	2.8	147.97	0.661	146.37	0.280	115.01	0.302	72.05	0.918	21.35	1.000
910	3.1	163.76	0.625	159.16	0.277	127.29	0.273	79.75	0.663	23.63	0.992
930	3.3	171.04	0.601	171.15	0.265	132.95	0.260	83.29	0.548	24.68	0.989
965	3.7	184.16	0.553	181.08	0.260	143.14	0.257	89.68	0.437	26.57	0.978
1000	3.85	197.76	0.534	193.31	0.255	153.71	0.244	96.30	0.390	28.54	0.975
1050	4.05	218.03	0.510	211.40	0.250	169.47	0.234	106.17	0.349	31.46	0.900
1095	4.3	237.12	0.480	232.34	0.245	184.31	0.231	115.47	0.319	34.22	0.866
1170	4.55	270.71	0.450	260.44	0.240	210.42	0.221	131.82	0.293	39.06	0.819
1260	4.9	313.96	0.407	301.51	0.235	244.04	0.215	152.89	0.272	45.30	0.738
1330	5.05	349.82	0.389	338.91	0.220	271.90	0.202	170.34	0.252	50.48	0.657
1400	5.1	387.61	0.383	375.26	0.205	301.28	0.202	188.75	0.240	55.93	0.579
1500	5.2	444.96	0.371	426.21	0.200	345.86	0.202	216.67	0.228	64.21	0.442
1600	5.6	506.26	0.323	486.23	0.200	393.51	0.202	246.53	0.220	73.05	0.389
1650	5.75	538.40	0.305	527.90	0.200	418.49	0.202	262.18	0.220	77.69	0.358
1680	5.75	558.16	0.305	551.70	0.200	433.84	0.202	271.80	0.217	80.54	0.344
1720	5.8	585.05	0.299	576.26	0.200	454.75	0.202	284.89	0.214	84.42	0.311
1805	5.87	644.31	0.290	624.94	0.200	500.80	0.202	313.75	0.211	92.97	0.274
1840	5.85	669.53	0.293	661.29	0.200	520.41	0.202	326.03	0.208	96.61	0.247
1900	5.95	713.91	0.281	699.41	0.200	554.91	0.202	347.64	0.208	103.02	0.241
1960	6	759.71	0.274	744.74	0.200	590.51	0.202	369.95	0.208	109.63	0.227
2000	6	791.04	0.274	780.80	0.200	614.85	0.202	385.20	0.208	114.15	0.219
2050	6	831.08	0.274	817.99	0.200	645.98	0.202	404.70	0.208	119.93	0.210
2100	6	872.12	0.274	858.71	0.200	677.88	0.202	424.68	0.208	125.85	0.205
2150	6	914.14	0.274	900.41	0.200	710.54	0.202	445.15	0.202	131.91	0.202
2205	6	961.51	0.274	946.03	0.200	747.36	0.202	468.21	0.202	138.75	0.202
2300	6	1046.15	0.274	1018.48	0.200	813.14	0.202	509.43	0.202	150.96	0.202
2400	6.1	1139.10	0.262	1108.71	0.200	885.39		554.69		164.37	
2600	6.1	1336.85	0.262	1272.21	0.200	1039.10		650.99		192.91	
3000	6.1	1779.84	0.262	1635.04	0.200	1383.42		866.70		256.83	
3300	6.2	2153.60	0.250	2031.43	0.200	1673.94		1048.70		310.77	
3500	6.6	2422.56	0.202	2334.64	0.200	1882.99		1179.67		349.58	

TABLE 3

TABLE 4 : BEREA SANDSTONE BA1 - DRAINAGE CAPILLARY PRESSURE CURVES

BEREA BA1 pore volume 7.04 cc

irreducible water saturation 0.347

RPM	water prod. volume (cc)	Pc at inlet face (mbar)	average water saturation	Pc curve by usual method: Pc (mbar)	Pc curve by usual method: S water	Pc curve from ultrasonic measurements: location N°3 (top) Pc (mbar)	location N°3 (top) S water	location N°2 (middle) Pc (mbar)	location N°2 (middle) S water	location N°1 (bottom) Pc (mbar)	location N°1 (bottom) S water
520	0	55.619	1.000	55.619	0.985	41.564	1.000	26.039	1.000	7.716	1.000
800	1	131.643	0.858	107.321	0.757	98.377	0.816	61.632	0.974	18.264	1.000
860	1.5	152.130	0.787	145.575	0.411	113.687	0.677	71.223	0.930	21.106	1.000
920	2	174.097	0.716	167.069	0.362	130.103	0.541	81.508	0.864	24.154	1.000
1000	2.5	205.692	0.645	195.584	0.355	153.714	0.424	96.300	0.710	28.537	1.000
1100	2.9	248.887	0.588	235.068	0.355	185.993	0.361	116.523	0.493	34.529	1.000
1200	3.2	296.196	0.545	281.061	0.354	221.348	0.354	138.672	0.424	41.093	1.000
1400	3.6	403.156	0.489	368.937	0.354	301.279	0.347	188.748	0.358	55.932	0.941
1620	3.9	539.817	0.446	496.097	0.354	403.406	0.350	252.729	0.358	74.892	0.883
1800	4	666.441	0.432	625.932	0.354	498.032	0.350	312.011	0.358	92.459	0.772
2100	4.2	907.100	0.403	830.109	0.347	677.877	0.347	424.682	0.361	125.847	0.600

TABLE 4

Figure 1 : Scheme of the experimental device : **1** Function generator ; **2** Amplifier ; **3** Channel scanner ; **4** Amplifier ; **5** Oscilloscope ; **6** Counter timer ; **7** Computer ; **8** Split ring assembly ; **9** Centrifuge bucket and core holder, sample to be centrifuged, ultrasonic transducers ; **10** Static reference sample ; **11** Thermal gauge ; **12** Digital thermometer ; **13** Centrifuge (modified commercial centrifuge). As received signals are very low, it is necessary to design devices having a very good electrical quality. This is obtained by adding amplifiers (2), (4) and by reducing electrical noises (we use coaxial wires and we earth some wires specifically).

Figure 2 : Simultaneous recordings during a centrifuge experiment (drainage of GV1 Vosges sandstone sample). In the lower part of the figure : (i) recording of the temperature as controlled by the centrifuge (thermal gauge) and, (ii) recording for a standard sample, i.e. a non-rotating, oil saturated sample fixed on the centrifuge bowl.

In the upper part of the figure, recordings for the rotating sample for different rotation velocities, at three locations along the core (see Fig. 1), bottom (No1), middle (No2) and top (No3). Vertical lines represent changes in the rotation velocity. Oscillations are due to thermal regulation (20°C+/- 3°C) and large variations to saturation changes.

Figure 3 : Test for the possibility of saturation changes when the centrifuge is stopped and after. Figure 3a : recordings of relative transit time variation ($\Delta t/to$) in a Vosges sandstone sample (GV4) at different velocity steps, 700, 750, 850 RPM , i.e. at early drainage stages. The centrifuge has been stopped after the two last steps and kept static for several hours after the last one. Figure 3b shows the signal variations after the sample GV1 has been rotated at 1000 RPM (advanced drainage stage) and at 1500 RPM (late drainage stage) and stopped during each step. Vertical lines represent changes in the rotation velocity. The sample was initially fully brine saturated and was centrifuged in oil.

Figure 4 :Test for the possibility of saturation changes when the centrifuge is stopped and after. Figure 4a and 4b show CT Scanner measurements of saturation, versus time, after a Vosges sandstone sample (GV6) has been centrifuged at 1020 RPM (advanced drainage stage) and 1500 RPM (late drainage stage) respectively. Saturation values are the average values for each slice of core in front of the 3 couples of ultrasonic transducers (see Fig. 1). Figure 4c presents saturation profiles along the core (i) at the beginning of a CT scanner analysis, 4 minutes

15 secondes after the 800 RPM and 2 minutes 30 secondes1020 RPM steps and, (ii) over the CT scanner analysis, 6 minutes 20 secondes to 54 minutes after the 1500 RPM step. Vertical bars present locations of ultrasonic transducers along the profile.

Figure 5 : Figure 5a : recordings of relative transit time variation ($\Delta t/to$) versus time for the 3 locations along GV6 Vosges sandstone core sample during centrifuging. The sample was initially fully saturated with brine progressively replaced by oil during the experiment (see Table 1). Vertical dashed lines indicate changes in rotation velocity step (800 to 3000 RPM). Blanks between the lines represent stops for CT scanner measurements of oil saturation values. At each rotation step, these values are measured for the core slices at the same locations of ultrasonic transducers. Figure 5b is the plot of these oil saturation values versus the corresponding plateau values for relative transit time variations, at the 3 locations of recording and for each rotation step. The dashed line represents our interpretation of "oil saturation / relative transit time variation" dependence.

Figure 6 : Plot of oil saturation values (CT Scanner meausrements) versus the corresponding plateau values for relative transit time variations, at the 3 locations of recording while centrifuging and for different rotation steps. Data are related to a drainage experiment for GV1 Vosges sandstone (Table 1) and for rotation velocity steps at 640, 750, 860, 950, 1060, 1350, 1500, 1750, 2100, and 3000 RPM. The dashed line represents our interpretation of "oil saturation / relative transit time variation" dependence.

Figure 7 : Plot of oil saturation values (CT Scanner meausrements) versus the corresponding plateau values for relative transit time variations, at the 3 locations of recording while centrifuging and for different rotation steps. Data are related to a drainage experiment for GV2 Vosges sandstone (Table 1) and for rotation velocity steps at 760, 920, 1100, 1300, 1500, 1700, 2200 and 2500 RPM. The dashed line represents our interpretation of "oil saturation / relative transit time variation" dependence.

Figure 8 : Recordings of relative transit time variation ($\Delta t/to$) versus time for the 3 locations along GV3 Vosges sandstone core sample during centrifuging. The sample was initially fully saturated with brine progressively replaced by oil during the experiment (see Table 1). Vertical dashed lines indicate changes in rotation velocity

step (from 560 to 3500 RPM). Note that the bottom of the sample is fully saturated with brine at least until 1220 RPM (no ultrasonic transit time changes for the No1 location of recording).

Figure 9 : Capillary pressure curves for oil / brine drainage in GV3 Vosges sandstone sample (see Table 1). The unfilled squares represent average saturation data as obtained in the standard centrifuge procedure. The dashed line is the capillary pressure curve as computed from these data (method by Forbes (1991) has been used). The dots are values directly obtained from our device : (i) the local oil saturation values are obtained directly from the transit time plateau values for each rotation velocity step, when assuming a linear correspondence between oil saturation and relative transit time variation (see text),

(ii) the corresponding capillary pressure values are calculated at each location of measurement assuming fluid equilibrium, the boundary condition and the continuity of fluid pathways (Pc=0 at end face ; $Pc=\frac{(\rho_{water}-\rho_{oil})}{2}\omega^2 (r^2 - r_{max}^2)$ at distance r from the axis, current hypotheses in the classical method).

Mercury injection data have been obtained independently on a twin sample and have been scaled with the usual procedure (Leverett, 1941 ; see Table 1).

Figure 10 : As in Figure 9 but for GV1 Vosges sandstone sample (see Table 1). The unfilled squares represent average saturation data as obtained in the standard centrifuge procedure (40 velocity steps from 390 to 3500 RPM have been performed, Table 3).

Figure 11 : As in Figure 9 but for BA1 Berea sandstone sample (see Table 1). The unfilled squares represent average saturation data as obtained in the standard centrifuge procedure (11 velocity steps from 520 to 2100 RPM have been performed, Table 4).

Table 1 : Core samples and fluids characteristics.

Table 2 : Centrifuge experiment results for oil/brine drainage capillary pressure curves of GV3 Vosges sandstone (see Table 1 and Figures 8 and 9). Capillary pressure values are calculated at inlet face and at each location of recording assuming fluid equilibrium, the boundary condition and the continuity of fluid pathways (Pc=0 at end face ; $Pc=\frac{(\rho_{water}-\rho_{oil})}{2}\omega^2 (r^2 - r_{max}^2)$ at distance r from the axis, current hypotheses in the classical

method). Corrected saturation and pressure for the standard interpretation are obtained following Forbes (1991). Local saturation values, at No 1, 2, 3 locations, are obtained directly from the transit time plateau values for each rotation velocity step, when assuming a linear correspondence between oil saturation and relative transit time variation (see text).

Table 3 : As in Table 2 but for GV1 Vosges sandstone (see Table 1 and Figure 10).

Table 4 : As in Table 2 but for GV3 Vosges sandstone (see Table 1 and Figure 11).

ABOUT THE AUTHORS

P. L. Forbes graduated as an engineer, from the "Ecole Polytechnique" (1978) and from the School of Mines of Paris (1981). He holds a Ph. D. in geology from Dijon University in 1987. He worked on economics surveys and mining projects before joining the "Institut Français du Pétrole" (IFP) in 1988. He was involved firstly in basin scale modeling for petroleum generation, expulsion and migration and, secondly in petrophysics studies. He is presently manager of the Reservoir Engineering Division with IFP in Rueil-Malmaison (France). He is a member of Society of Core Analysts and of European Association of Petroleum Geoscientists and Engineers.

Catherine Chardaire-Rivière is a Research Engineer at the Institut Français du Pétrole. Her expertise includes numerical studies of multiphase flows in porous media and Magnetic Resonance Imaging applied to fluids in porous media. She holds a degree from the Ecole Nationale Supérieure d'Informatique et de Mathématiques Appliquées of Grenoble (1983). She is a member of Society of Core Analysts.

Françoise Deflandre is a Physicist at the Institut Français du Pétrole. She obtained a degree in physical measurements in 1979. Her current duties include research works and measurements on fluid flow in porous media. She is presently involved in studies on ultrasonic wave behavior and in applications for static or dynamic measurement of fluid saturation in porous media.

Marc Fleury is a Physicist from the "Ecole Polytechnique Fédérale de Lausane" (1983). He holds a PhD in Fluid Mechanics from the "Institut de Mécanique de Grenoble". He spent three years in USA and Canada as a research Assistant.He was mainly involved in the study of mixing processes (turbulence, double diffusion) and their applications to the ocean. He is a member of American Geophysical Union.

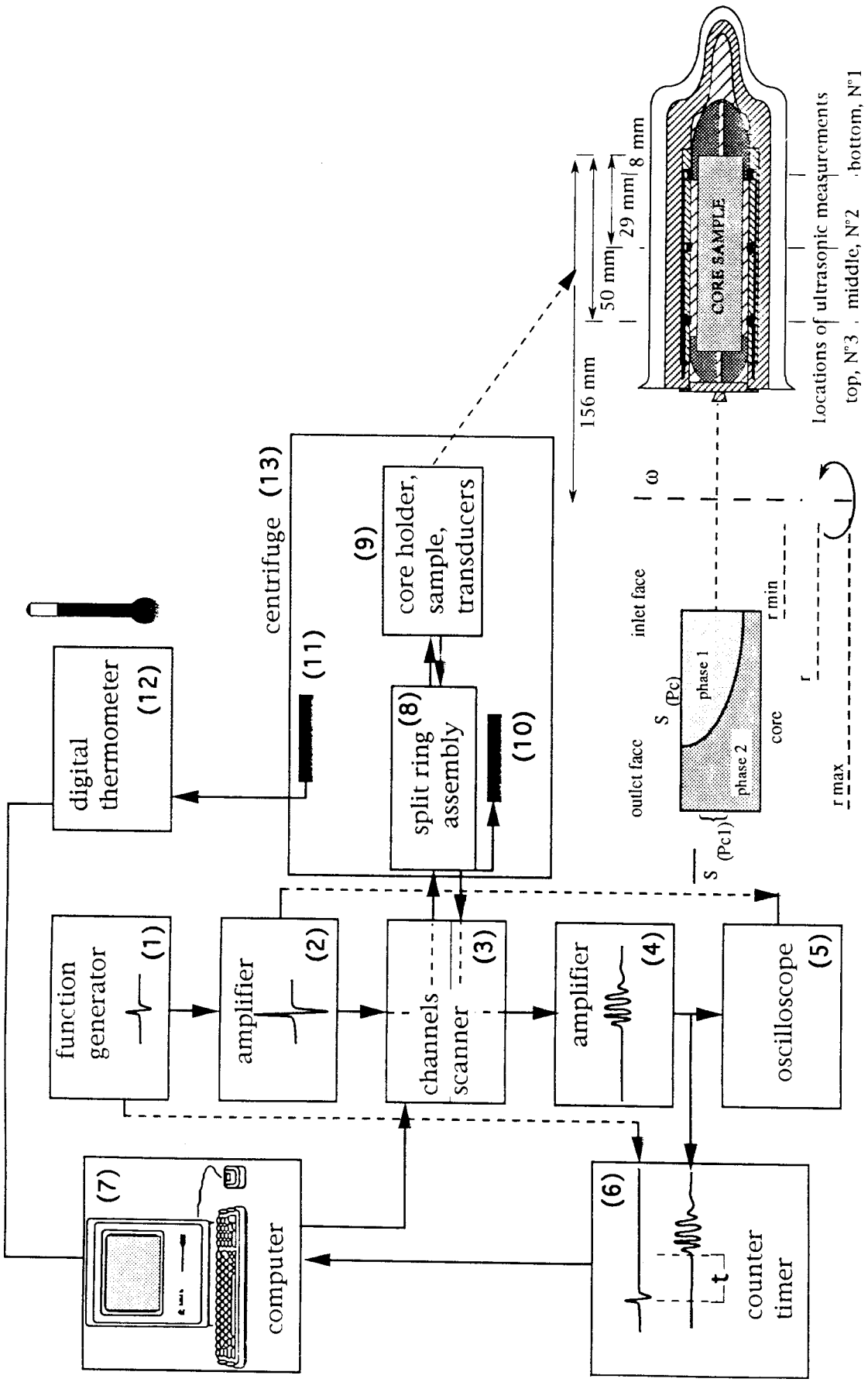
function generator (1)
amplifier (2)
channels scanner (3)
amplifier (4)
oscilloscope (5)
counter timer (6)
computer (7)
split ring assembly (8)
core holder, sample, transducers (9)
(10)
(11)
centrifuge (13)
digital thermometer (12)
156 mm
50 mm
29 mm
8 mm
CORE SAMPLE
Locations of ultrasonic measurements
top, N°3 . middle, N°2 . bottom, N°1
ω
inlet face
outlet face
S (Pc)
phase 1
phase 2
core
r min
r max
r
S (Pc1)

FIGURE 1

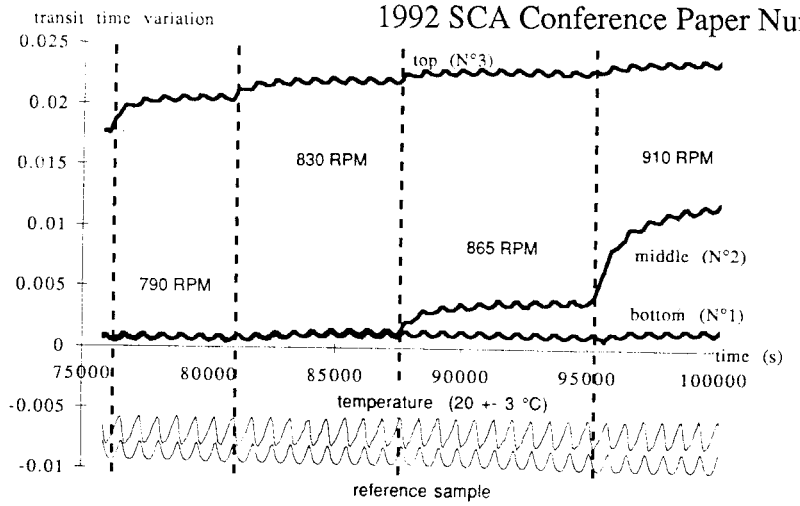

FIGURE 2

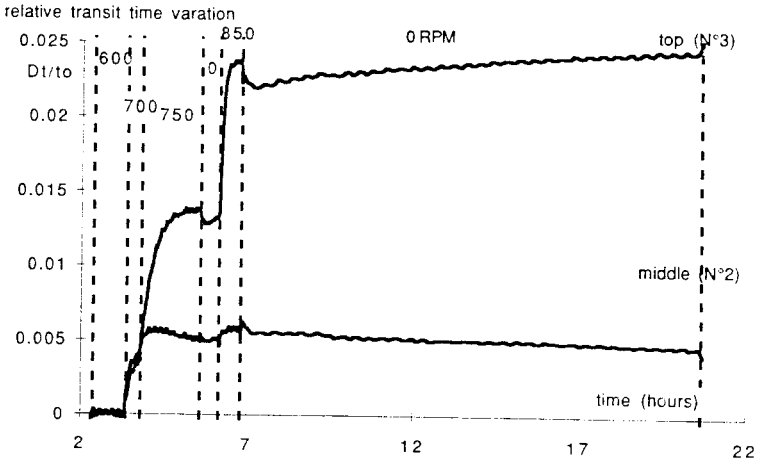

FIGURE 3a

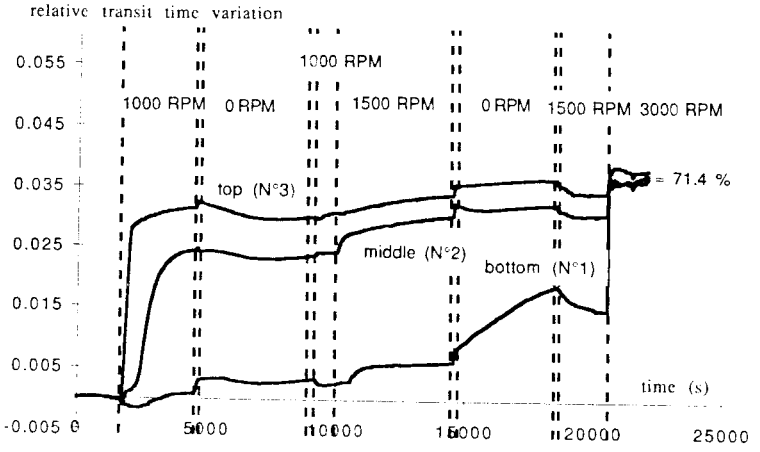

FIGURE 3b

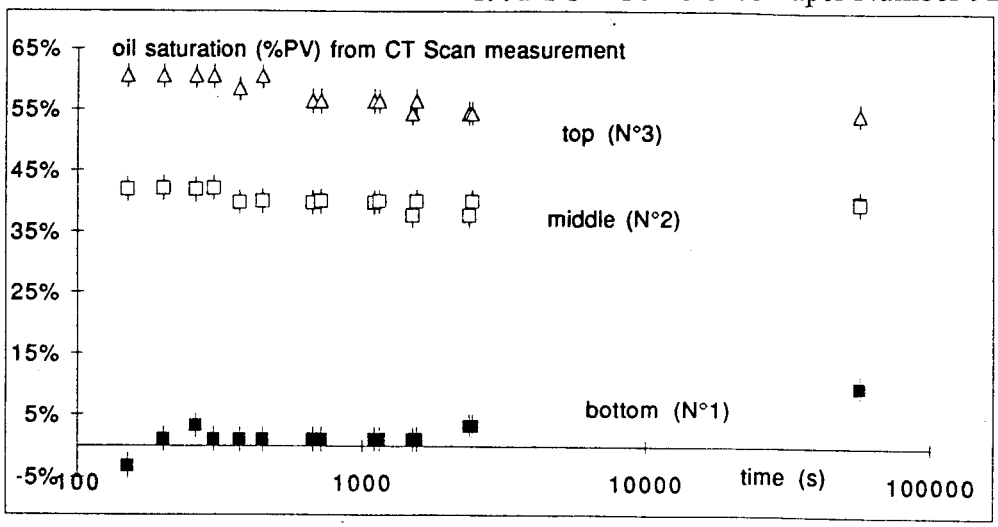

FIGURE 4a

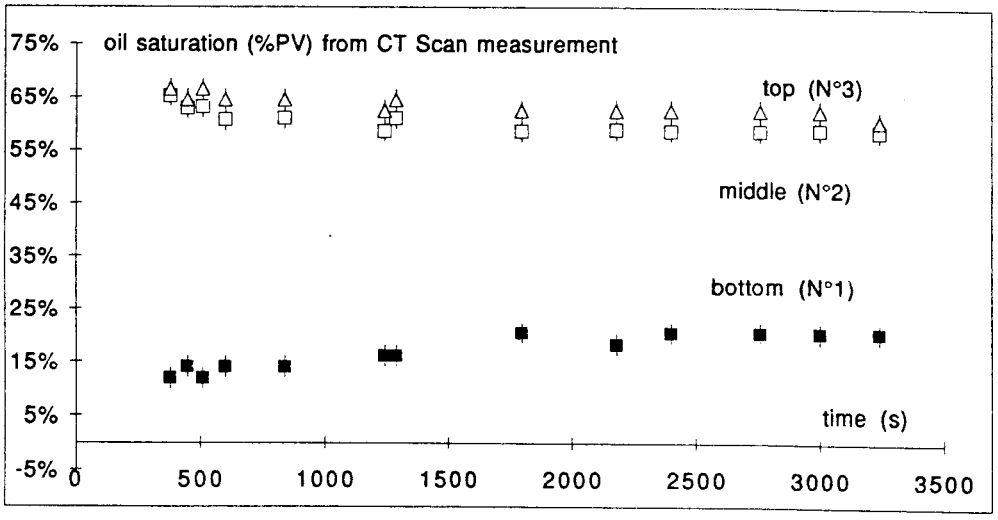

FIGURE 4b

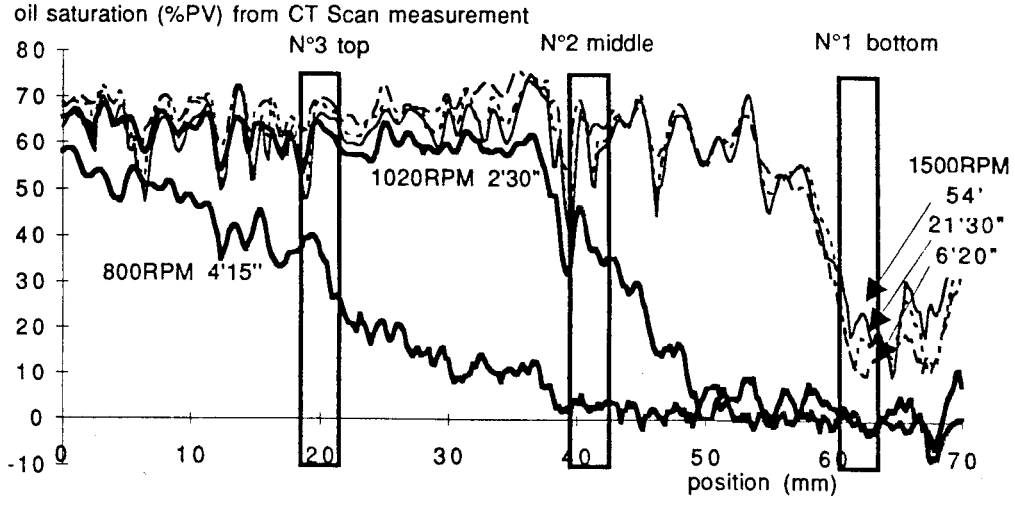

FIGURE 4c

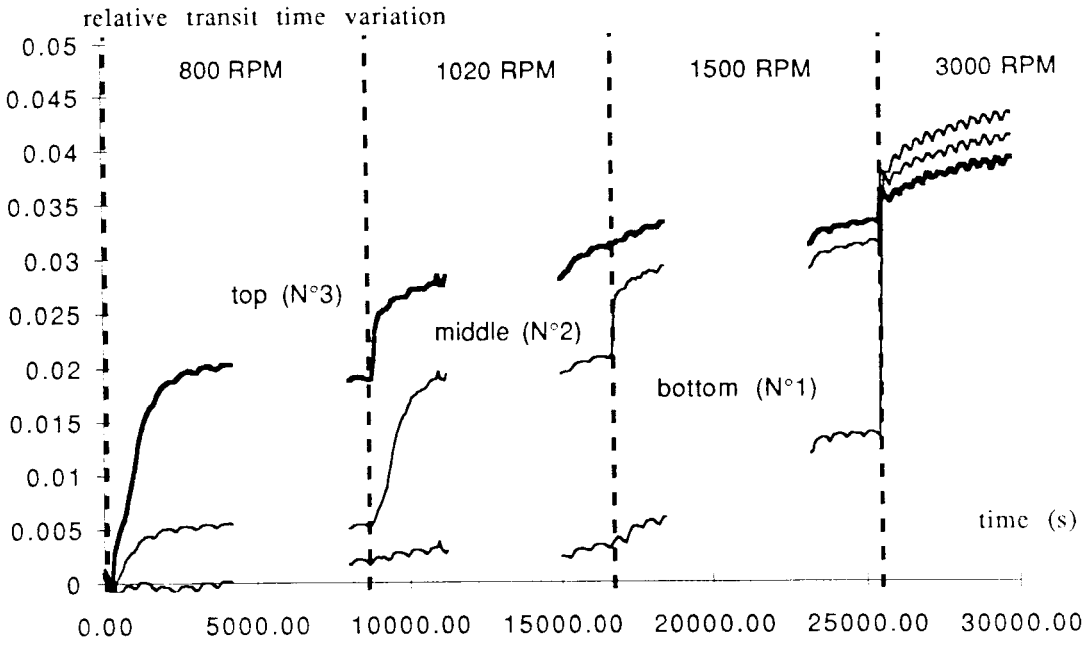

FIGURE 5a

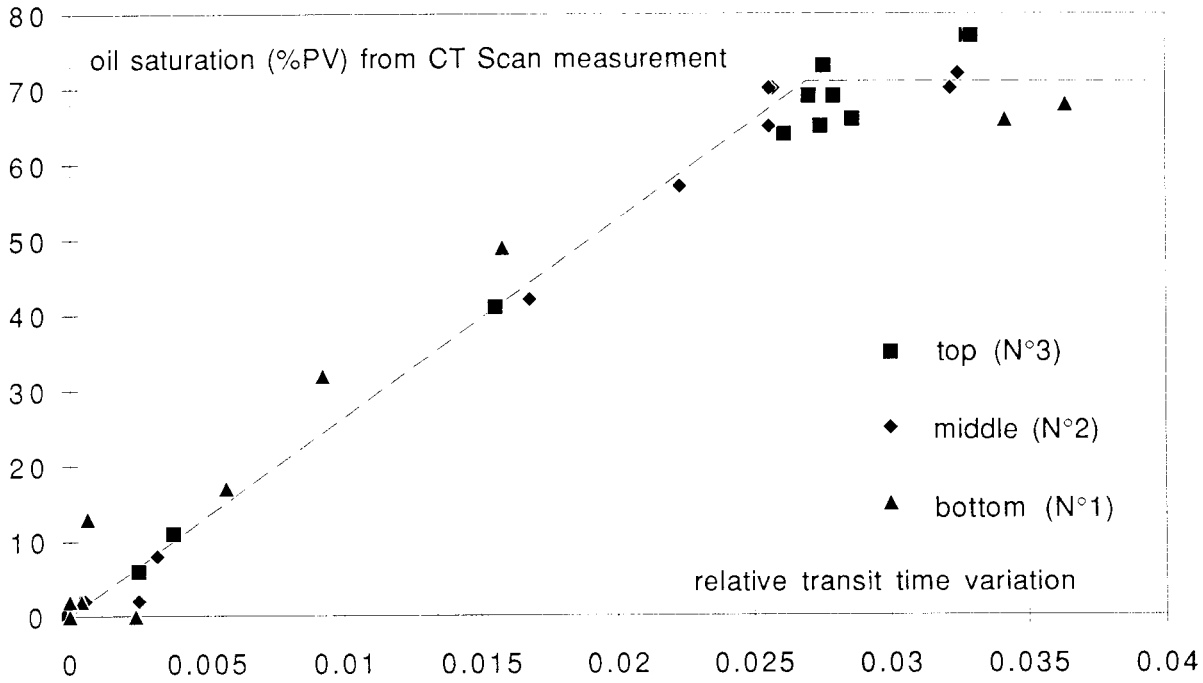

FIGURE 6

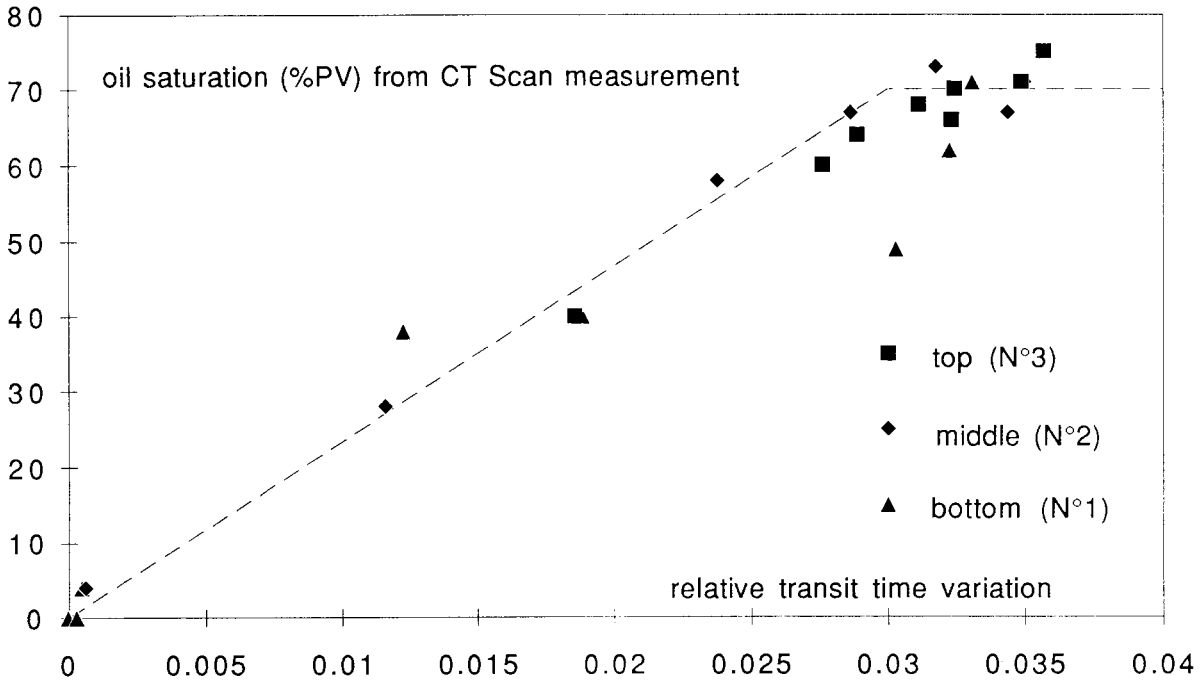
oil saturation (%PV) from CT Scan measurement
relative transit time variation
top (N°3)
middle (N°2)
bottom (N°1)
80
70
60
50
40
30
20
10
0
0
0.005
0.01
0.015
0.02
0.025
0.03
0.035
0.04

FIGURE 7

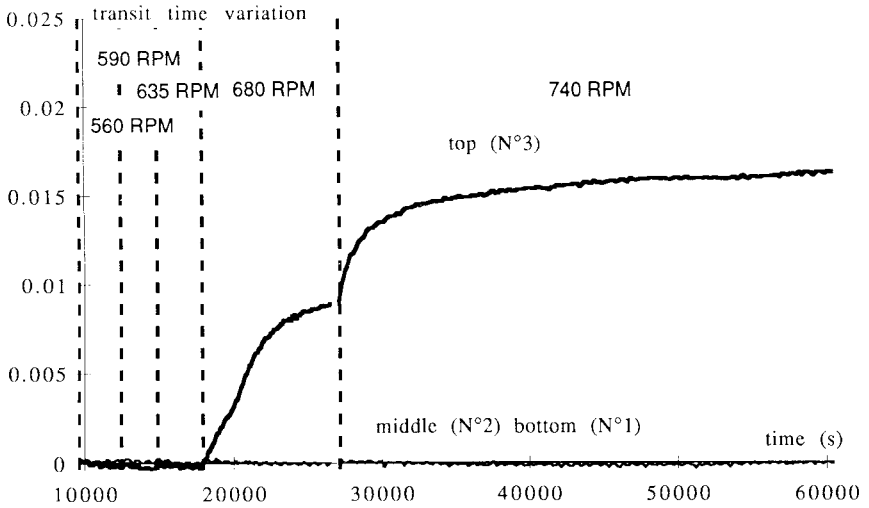

FIGURE 8a

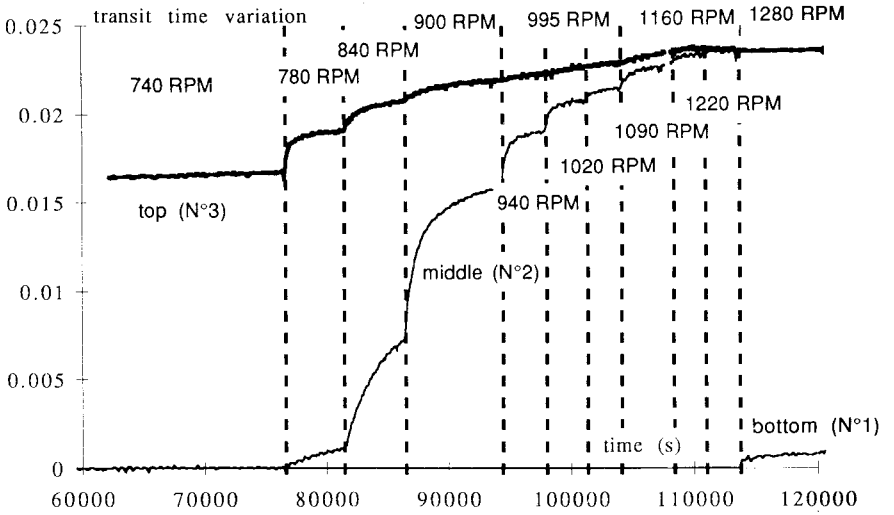

FIGURE 8b

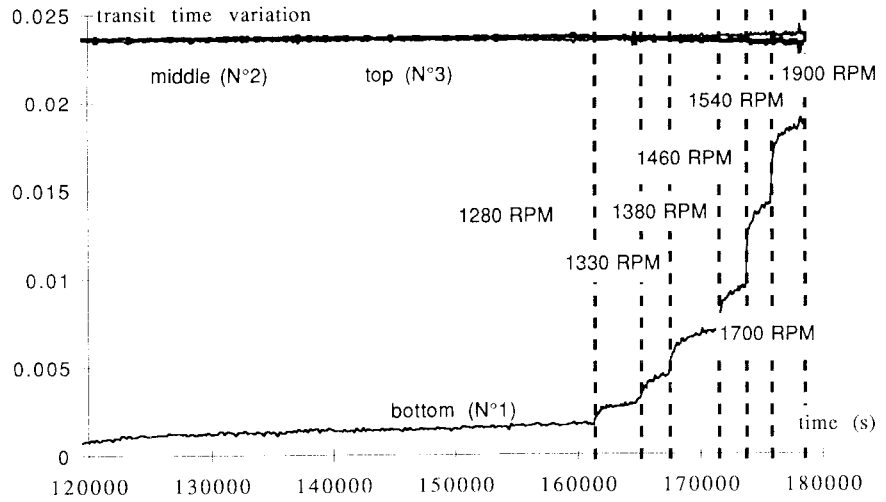

FIGURE 8c

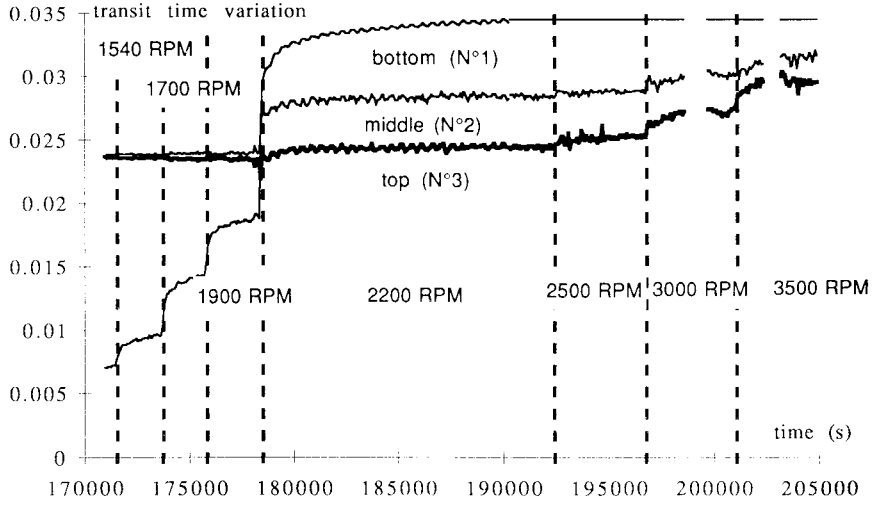

FIGURE 8d

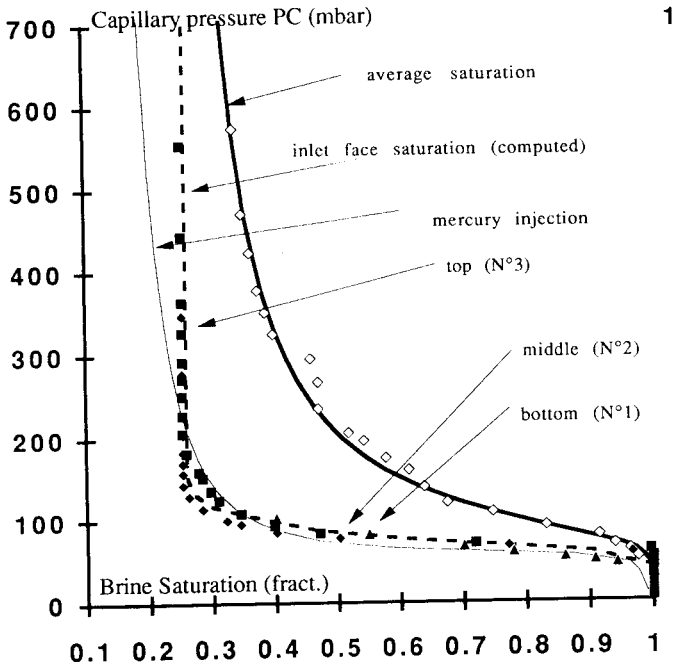

FIGURE 9

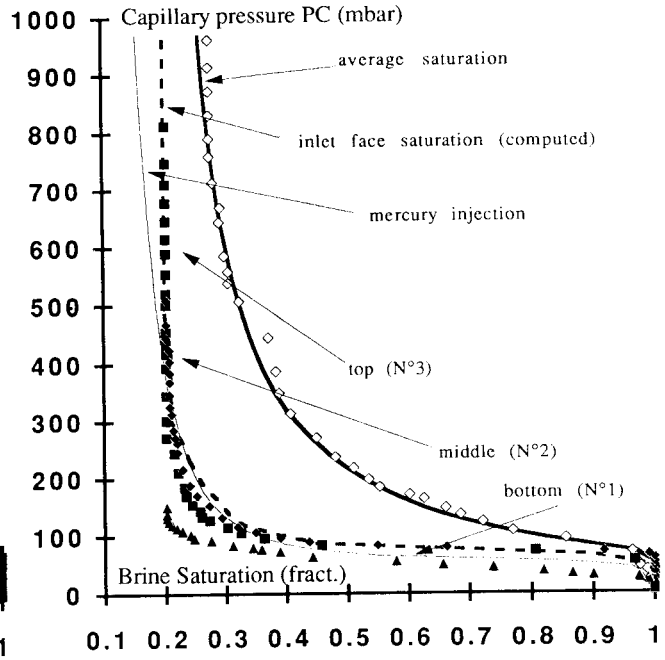

FIGURE 10

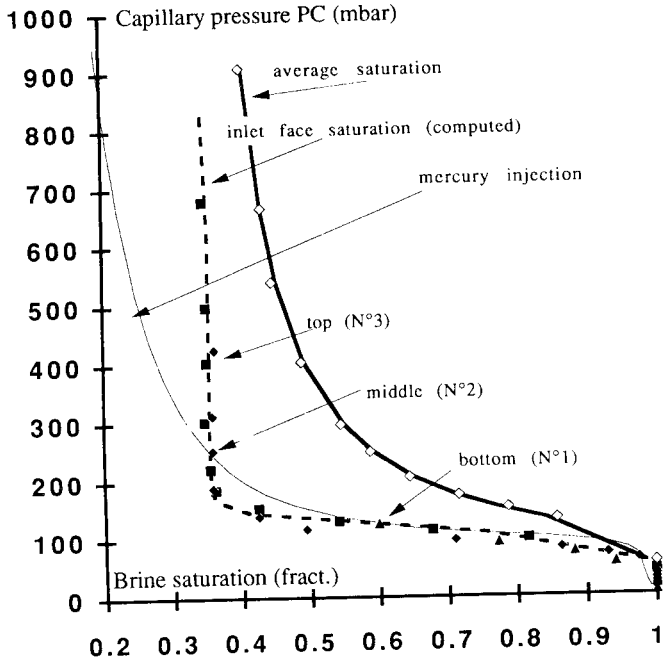

FIGURE 11